An improved Cauchy robust correction-sage Husa extended Kalman filtering algorithm for high-precision SOC estimation of Lithium-ion batteries in new energy vehicles.

ZHU, C., WANG, S., YU, C., ZHOU, H., FERNANDEZ, C. and GUERRERO, J.M.

2024

An Improved Cauchy Robust Correction-Sage Husa Extended Kalman Filtering Algorithm for High-precision SOC Estimation of Lithium-ion Batteries in New Energy Vehicles

Chenyu Zhu[a], Shunli Wang[a*], Chunmei Yu[a], Heng Zhou[a], Carlos Fernandez[b], Josep M. Guerrero[c]

[a]School of Information Engineering, Southwest University of Science and Technology, Mianyang 621010, China; [b]School of Pharmacy and Life Sciences, Robert Gordon University, Aberdeen AB10-7GJ, UK; [c]Department of Energy Technology, Aalborg University, Pontoppidanstraede 111 9220 Aalborg East, Denmark.

Abstract: The accurate estimation of battery State of Charge (SOC) is a key technology in the research of electric vehicle battery management systems. In order to solve the problem of inaccurate noise estimation in nonlinear systems, an improved Cauchy robust correction-Sage Husa extended Kalman filtering (CRC-SHEKF) algorithm is proposed for high-precision SOC estimation of lithium-ion batteries in new energy vehicles. Considering the polarization effect of the battery, the FFRLS algorithm is used for online parameter identification of the Dual Polarization model. Using robust data correction methods, the Cauchy robust function is simplified for real-time correction of the covariance matrix Q of system state noise and the covariance matrix R of the observed noise in the filtering process and combined with SHEKF for SOC estimation. The experimental results show that under different temperature conditions and complex working conditions, the proposed CRC-SHEKF algorithm has the minimum mean absolute error (MAE), root mean square error (RMSE), and maximum error (MAX). Under the condition of the Beijing bus dynamic stress test (BBDST) at 15℃, the MAE, RMSE, and MAX of the CRC-SHEKF algorithm are 0.392%, 0.716%, and 0.945%, with the computing time of only 4.839 seconds. The algorithm proposed in this article has high accuracy and robustness, and has practical application value, providing a reference for the application of lithium battery condition monitoring.

Key words: Lithium-ion battery; SOC; Cauchy robust correction; Sage Husa extended Kalman filtering; Dual Polarization model

***Corresponding author**: Shun-Li Wang. Tel: +86-15884655563. E-mail address: wangshunli@swust.edu.cn.

Highlights:

- The Dual Polarization model is established and the FFRLS is used for online parameter identification.
- An improved Cauchy robust correction-Sage Husa extended Kalman filtering algorithm is proposed.
- Simplified Cauchy robust function for real-time correction of system noise during filtering process.
- The MAE, RMSE, and MAX of complex BBDST working conditions are 0.392%, 0.716%, and 0.945%.

1. Introduction

With the global energy crisis and the aggravation of climate warming, more and more attention has been paid to the research on electric vehicles [1]. Power batteries are an essential core in electric vehicles and determine the development of the new energy vehicle industry [2]. Lithium-ion batteries have many advantages, including high energy density, long cycle life, no memory effect, and low self-discharge rate. Therefore, it is widely used in electric vehicles [3]. Although lithium-ion batteries have a wide range of applications, there are still issues with their safety and lifespan. In recent years, the spontaneous combustion of electric vehicles has prevented them from gaining public recognition and popularity [4]. To avoid safety accidents, the Battery Management System (BMS) is required to control the battery and monitor various parameters and battery status changes within the battery [5]. In particular, the state of charge (SOC) of the battery indicates the remaining power of the power battery [6]. It is one of the important parameters to characterize the battery status. Accurate estimation of SOC is critical for batteries [7; 8]. During the actual operation of the battery, BMS will allocate SOC to different systems, making the control efficiency of electric vehicles the highest.

Early commonly used SOC estimation algorithms include the ampere-hour measurement method, open-circuit voltage method, neural network method, Kalman filter algorithm, etc. The ampere-hour measurement method has been widely used because of its simple principle and convenient calculation [9]. However, the performance of the ampere-hour measurement method is highly dependent on the measurement accuracy of the current. In practice, this open-loop calculation method will cause error accumulation due to the lack of automatic error correction ability and the interference of uncertain factors. This method is usually combined with other algorithms because of its low estimation accuracy. The open-circuit voltage method is usually used in conjunction with the ampere-hour measurement method [10; 11]. It is usually used to calibrate or obtain the initial SOC value of the battery. However, due to its high measurement cost and time-consuming

nature, it is not commonly used for online estimation. The neural network method is based on the black box model to describe the strong nonlinear relationship between input and output variables [12]. It also requires a lot of high-fidelity data to support, but the collection of these data will be costly [13]. Kalman filter algorithm is a typical optimal estimation algorithm, which is generally used in linear systems [14; 15]. When the statistical characteristics of noise are known, the algorithm has high estimation accuracy. However, the battery is a typical nonlinear system, and it is difficult to accurately obtain its noise statistical characteristics. Therefore, scholars have improved the Kalman filter algorithm. The extended Kalman filtering algorithm converts a non-linear system into a linear system using a Taylor formula [16; 17]. The use of approximation can effectively solve the nonlinear problem of battery systems, but it is still affected by random noise. For most complex nonlinear systems, the accurate acquisition of noise variance is a difficult problem [18]. Numerous experiments have shown that when the noise estimation is inaccurate, especially when the process noise estimation is too large, the filtering accuracy will decrease, and even lead to filtering divergence [19].

Due to issues such as inaccurate noise estimation and filtering divergence, the estimation results may not be ideal. Therefore, many scholars have proposed some improvement methods to solve this problem. It is mainly divided into two categories: one is the real-time estimation of noise, and the other is robust Kalman filters. The first method can add noise to the state vector to update the noise in real-time, but this method has certain limitations, as its process noise estimation is inaccurate and the deviation is small. Another example is to derive an estimation equation for noise statistical characteristics using an improved Sage Husa estimator [20; 21], maximum likelihood estimation [22; 23], and maximum expectation rule, combined with the EKF algorithm for real-time updates. It can effectively solve the EKF filtering problem in the presence of unknown noise. The second method is the robust Kalman filter. It can ensure the performance of state estimation error when the noise variance is uncertain. For example, based on the unscented Kalman filter (UKF), some scholars proposed a robust unscented Kalman filter based on the H infinite norm [24]. This algorithm improves the

simplified UKF in Krein space and changes the filtering gain through specific parameter parameters, making the filtering effect more robust [25]. In addition, some scholars have updated the calculation formula of the state error variance matrix P. Changing the original subtraction to addition avoids the problem of an undetermined variance matrix caused by positive definite matrix subtraction operations. After experimental verification, this method can achieve better filtering accuracy requirements compared to the traditional UKF algorithm. In order to overcome the divergence or accuracy degradation of UKF in high-dimensional state space, some scholars have proposed the Cubature Kalman Filter (CKF). However, due to the influence of uncertain prior noise, the estimation accuracy is not high [26].

In the literature [27], the method based on the adaptive extended Kalman filter (AEKF) is used to realize SOC estimation. The adaptive method is added to the noise estimation process to update the process and measure the noise covariance matrix, which improves the estimation accuracy. However, the above literature can not update the battery model parameters in real-time. It belongs to the offline parameter identification method [28]. To avoid this shortcoming, the literature [29] uses AEKF and recursive least squares (RLS) to update the model parameters in real-time [30]. It belongs to the online parameter identification method. Due to its closed-loop feedback structure [31], it has better accuracy of SOC estimation than the first method. The above methods mentioned that offline parameter identification and online parameter identification are the two main methods of parameter identification related to the battery mathematical model [32; 33]. The parameters inside the battery are related to many factors, such as aging, temperature, etc. At this time, it is difficult to characterize the parameter changes with the same formula [34; 35]. The results of offline parameter identification are fixed values, which do not characterize the intense chemical reactions inside the battery. The online parameter identification method can calculate the parameters of the battery model in real-time and simulate the changes in the internal parameters of the battery [36]. The accuracy of the estimation result is improved effectively by participating in the closed-loop feedback through the SOC estimation result [37; 38].

The forgetting factor recursive least square algorithm (FFRLS) is a commonly used online parameter identification method, which improves the data saturation problem of the RLS algorithm when identifying time-varying parameters [39]. The forgetting factor is added to adjust the weight ratio between time t and time t-1 [40]. When the new data fails to meet the expected correction and recognition results, it is necessary to reduce the impact of the old data and assign higher weights to the new data. This makes the FFRLS algorithm sensitive to changes in input process features and able to respond quickly.

In the presence of non-Gaussian noise, a simple Kalman filtering method cannot guarantee the accuracy of SOC estimation. The literature [41] proposes the adaptive kernel width-based maximum correntropy criterion-adaptive iterative extended KF (AMCC-AIEKF) algorithm for estimating SOC. This method combines the Maximum Correlation Criterion (AMCC) of Adaptive Kernel Width with the Levenberg Marguard (L-M) principle. Replace the minimum mean square error (MMSE) criterion with the MCC criterion, and use an L-M optimized multi-step iterative filter to update the covariance matrix and state of AMCC correction to achieve SOC estimation. The MAE and RMSE of the proposed AMCC-AIEKF algorithm are 1.2455% and 0.5434%, respectively. However, this literature only analyzed the first-order RC equivalent circuit model, and its SOC estimation accuracy is not high enough under complex noise conditions. The literature [42] proposes four weighted state fusion robust Kalman estimators (filters, predictors, and smoothers). Using the augmented state method and virtual noise technology, transform the original system into a system with uncertain noise variance. Based on the principle of minimax robust estimation, design a unified form of robust filters and smoothers. The effectiveness of the proposed method was verified through a simulation example of a power system. This method is mainly aimed at robust weighted state fusion estimation of time-varying multi-sensor network systems with mixed uncertainty. The method proposed in this literature can be applied to the SOC estimation problem of lithium batteries.

For most nonlinear systems, the statistical characteristics of noise are difficult to obtain accurately. In order

to solve the problem of inaccurate noise estimation, this paper proposes an improved estimation error processing method: Cauchy robust correction. Combining the Sage Husa adaptive method, an improved Cauchy robust correction-Sage Husa extended Kalman filtering (CRC-SHEKF) algorithm is proposed to estimate the SOC of lithium-ion batteries. In this paper, with the method of robust data correction, the minimum point of the robust objective function corresponds to the minimum point of the residual between the measured estimated value and the actual value. Based on the residual between the measured prior value and the actual value, the joint weight function is used to correct the noise estimate in the filtering process in real-time. It reduces the weight of the inaccurate estimate of noise, minimizes the robust objective function, and improves the filtering accuracy of the SHEKF algorithm. The covariance matrix Q of system state noise is dynamically modified by the simplified Cauchy robust function. Considering the influence of SOC interval on the battery, the covariance matrix R of the observed noise is dynamically adjusted. The problems of system noise caused by unknown statistical characteristics and battery model estimation accuracy degradation are solved. The Cauchy robust correction process uses judgment statements to correct noise, simplifying the iterative calculation process and reducing computation time. Combined with FFRLS online parameter identification method, the identified battery model parameters are transmitted to the CRC-SHEKF algorithm in real time to estimate the SOC, making the SOC estimation more accurate and reliable. This method is more adaptable to environments with uncertain random noise, suitable for different temperatures and complex working conditions, and has a shorter calculation time. It can improve the accuracy and robustness of SOC estimation for lithium batteries, and has practical application value, providing a reference for the application of lithium battery condition monitoring.

2. Mathematical analysis

2.1. Dual Polarization model

For model-based forecasting methods, the accuracy and complexity of the model are crucial. The battery models used for state estimation are divided into three types: electrochemical model, neural network model, and

equivalent circuit model (ECM). ECM is widely used in SOC estimation because of its simple structure, centralized parameters, small computation, clear physical meaning, and high accuracy of voltage fitting. The common battery ECM is basically included in the model with n-order RC. The model with 0-order RC is the Rint model, the first-order RC is the Thevenin model, and the second-order RC is the DP model. The research shows that as the number of RC networks increases, the mathematical expression of the model becomes more complex. Too many RC networks will make it more difficult to identify parameters and estimate the SOC of the model, which is not conducive to the calculation of the battery management system. In this paper, the Dual Polarization model is built as the equivalent circuit model of batteries. It can simulate concentration polarization and electrochemical polarization separately so that it can accurately simulate the dynamic characteristics of batteries. The first RC network represents the electrochemical polarization of the battery. When a certain amount of external current passes through the electrode, the transfer of electrons per unit time cannot participate in the oxidation-reduction reaction promptly, resulting in excess charges on the electrode surface and causing the electrode potential to deviate from its equilibrium potential. This phenomenon of electrode potential deviating from equilibrium potential due to insufficient rapid electron gain and loss, which hinders the reaction on the electrode surface, is called electrochemical polarization. The second RC network represents the concentration polarization of the battery. Concentration polarization is caused by the sluggishness of ion mass transfer processes. The concentration difference caused by the lack of timely replenishment of reactants in the liquid layer near the electrode surface or the delayed evacuation of products has led to potential deviation.

Compared with other equivalent models, it can better characterize the time-varying characteristics of the internal parameters of lithium batteries, and the SOC estimation accuracy is higher. While the polarization capacitance and polarization resistance characteristics are satisfied, the complexity of the model is controlled within a reasonable range. Therefore, the Dual Polarization model is selected according to the above judgment that is shown in Fig. 1.

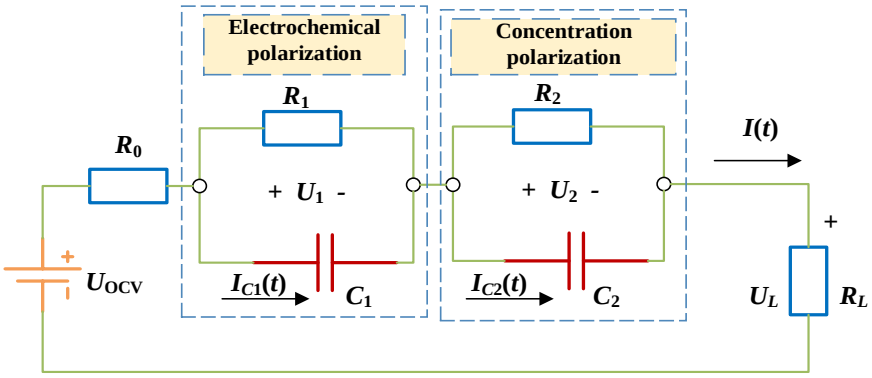

Fig. 1 Dual Polarization model

R_0 is the equivalent internal resistance of the battery model, R_1 is the internal resistance of polarization caused by the battery polarization effect, and R_2 is the internal resistance of polarization caused by the battery concentration polarization effect. C_1 and C_2 are polarized capacitors. The first RC network describes the impedance of transmission between electrodes, and the second RC network describes the impedance of lithium-ion diffusion in electrode materials. U_0 is the voltage divided by R_0. U_1 and U_2 are voltage when resistors R_1 and R_2 are current I. U_{OCV} is open circuit voltage and U_L is output terminal voltage. According to Kirchhoff's Law of Voltage and Current, the expressions of the voltage and current of the equivalent circuit are shown in Eq. (1).

$$\begin{cases} U_L = U_{OCV} - U_0 - U_1 - U_2 \\ I = \dfrac{U_0}{R_0} = \dfrac{U_1}{R_1} + C_1 \dfrac{dU_1}{dt} = \dfrac{U_2}{R_2} + C_2 \dfrac{dU_2}{dt} \end{cases} \tag{1}$$

The output voltage and current can be obtained through HPPC charging and discharging tests as inputs for the identification system. The parameter values of R_0, R_1, R_2, C_1, and C_2 need to be identified by the parameters.

The SOC is an indicator used to reflect the remaining power of a battery. Its numerical value is defined as the ratio of remaining capacity to battery capacity, which is related to the charging and discharging time and current of the battery in use. It is a highly valuable indicator for inferring the current battery life. The calculation expression for SOC is shown in Eq. (2).

$$SOC(k) = SOC(k_0) - \frac{\int_0^k I(k)\eta dk}{Q_0} \tag{2}$$

Wherein, $SOC(k_0)$ is the initial SOC value of the battery, Q_0 is the capacity of the battery and η is the Coulomb efficiency for charging and discharging. Combined with the SOC definition, the discrete state-space equation can be obtained as shown in Eq. (3).

$$\begin{bmatrix} SOC_{k+\Delta k} \\ U_{1,k+\Delta k} \\ U_{2,k+\Delta k} \end{bmatrix} = \begin{bmatrix} 1 & 0 & 0 \\ 0 & e^{-\frac{\Delta k}{\tau_1}} & 0 \\ 0 & 0 & e^{-\frac{\Delta k}{\tau_2}} \end{bmatrix} \begin{bmatrix} SOC_k \\ U_{1,k} \\ U_{2,k} \end{bmatrix} + \begin{bmatrix} -\frac{\eta \Delta k}{Q_0} \\ R_1(1-e^{-\frac{\Delta k}{\tau_1}}) \\ R_2(1-e^{-\frac{\Delta k}{\tau_2}}) \end{bmatrix} I(k) + \omega(k) \tag{3}$$

In Eq. (3), $\tau_1 = R_1C_1$ and $\tau_2 = R_2C_2$. ω is the state error, which is the zero-mean white noise of the covariance matrices Q. After discretization, its initial state equation is shown in Eq. (4).

$$U_{L,k} = U_{OCV,k} - R_{1,k} I(k) + \begin{bmatrix} 0 & -1 & -1 \end{bmatrix} \begin{bmatrix} SOC_{k+\Delta k} \\ U_{1,k+\Delta k} \\ U_{2,k+\Delta k} \end{bmatrix} + v(k) \tag{4}$$

In Eq. (4), Δk is the sampling time interval. v is the measurement error, which is the zero-mean white noise of the covariance matrices R.

2.2. Parameter identification

Establishing an appropriate equivalent model for battery characteristics is the basis for accurately estimating SOC. Therefore, it is necessary to select appropriate parameter identification methods based on different situations. Parameter identification methods are mainly divided into two categories: online parameter identification and offline parameter identification. The principle of the offline parameter identification method is to calculate internal parameters through mathematical expressions of voltage, current, and internal parameters during each discharge process. But these parameters do not have time-varying characteristics, and the battery undergoes different changes with aging, temperature, etc. It cannot characterize the dynamic changes that occur

inside the battery due to intense chemical reactions. The online parameter identification algorithm can effectively solve the above problems. The online parameter identification method is to estimate the parameter identification value by combining the acquired data and revising the result of the previous time so that the parameter identification result at each time is in high conformity with the actual model.

2.2.1. Forgetting factor recursive least square algorithm

The forgetting factor recursive least squares (FFRLS) algorithm is a parameter identification method based on recursive least squares (RLS) with the forgetting factor. It is suitable for large-scale datasets and situations that require real-time computation. The forgetting factor can adjust the weights of old and new data to reduce the impact of previous data on current calculations and avoid data saturation issues. The basic idea of the FFRLS is to use a recursive formula to correct the predicted value of the previous time for each new set of data measured during system operation to obtain the estimated parameter value at the current time. The principle of the FFRLS method is simple and can be applied to static and dynamic systems, linear systems, and nonlinear systems. This algorithm has the ability to respond quickly to changes in input process characteristics. The system equations of the FFRLS algorithm are shown in Eq. (5) to Eq. (8).

The identified parameter expression is shown in Eq. (5).

$$\hat{\theta}(k)=\hat{\theta}(k-1)+K(k)\left[y(k)-\phi(k)\hat{\theta}(k-1)\right] \tag{5}$$

The algorithmic gain matrix is shown in Eq. (6).

$$K(k)=P(k-1)\,\phi(k)\left[\lambda+\phi^{T}(k)P(k-1)\,\phi(k)\right]^{-1} \tag{6}$$

The covariance matrix is shown in Eq. (7).

$$P(k)=\frac{1}{\lambda}\left[I-K(k)\phi^{T}(k)\right]P(k-1) \tag{7}$$

The system error expression is shown in Eq. (8).

$$e_0(k) = y(k) - \phi(k)\hat{\theta}(k-1) \tag{8}$$

Wherein, $\hat{\theta}(k)$ is the estimated value of the identified parameter at time k, $\phi(k)$ is the system input, $y(k)$ is the system output. λ is the forgetting factor. The forgetting factor is the weight ratio of the previous moment to the next. When the new data can not correct the identification results, it is essential to reduce the weight of the old data and increase the role of the new data. The value range of λ is $0 < \lambda \leq 1$. In this paper, $\lambda = 0.98$.

2.2.2. OCV-SOC curve fitting of hysteresis effect

The terminal voltage of the lithium-ion battery after standing for a period of time is called the open-circuit voltage (OCV). There is a certain mathematical relationship between OCV and SOC. Taking the ternary lithium-ion battery as the research object, the HPPC test was carried out on the lithium-ion battery. The discharge test steps are as follows: first, fully charge the battery with standard constant current and voltage; Set aside for 1 hour; 1C constant current discharge for 10 seconds; Set aside for 40 seconds; 1C constant current charging for 10 seconds; Set aside for 10 minutes; Discharge from 1C constant current for 12 minutes to reduce SOC by 0.1; Set aside for 40 minutes; Starting from the 1C constant current discharge step, repeat the discharge and charging steps. Considering the battery hysteresis effect, the charging experiment is conducted in the same way. In the charge test and discharge test, record the corresponding OCV value for each 10% decrease or increase in SOC. And calculate the average OCV of charge and discharge test. Under HPPC testing at 15 ℃, the corresponding relationship between SOC and OCV is shown in Tab. 1.

Tab. 1 The corresponding relationship between SOC and OCV

SOC(%)	Discharge test OCV(V)	Charge test OCV(V)	Average OCV(V)
100	4.1840	4.1889	4.18645
90	4.0324	4.0593	4.04585
80	3.9228	3.9530	3.93790
70	3.8232	3.8538	3.83850
60	3.7250	3.7366	3.73080
50	3.6502	3.6672	3.65870

40	3.6125	3.6278	3.62015
30	3.5612	3.5965	3.57885
20	3.5276	3.5416	3.53460
10	3.4578	3.4728	3.46530

Hysteresis is a complex dynamic behavior of batteries, especially those based on embedded materials. The hysteresis effect of the battery is mainly reflected in that, depending on the previous state of charge or discharge, the battery has a different balance potential even under the same SOC state. Because of the hysteresis effect, the OCV value of the battery is a single-value function of the battery SOC value and is also affected by the battery charging or discharging history, which makes the same SOC may have different OCV values. The OCV-SOC curve will form a banded hysteresis structure with gaps at both ends. The OCV-SOC fitting curve of the hysteresis effect is shown in Fig. 2.

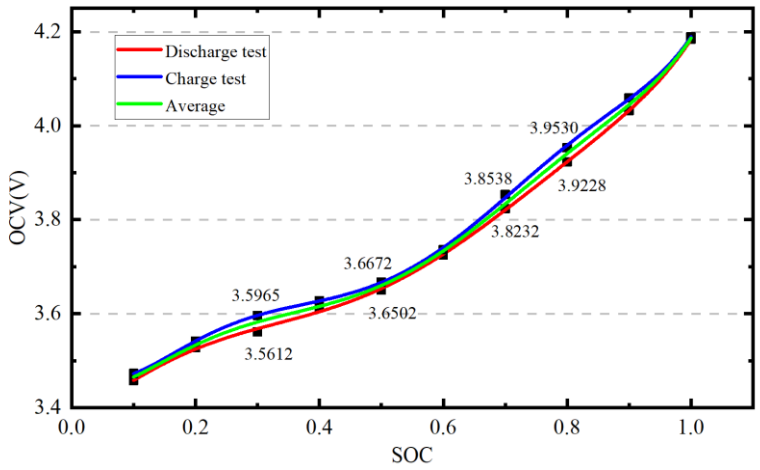

Fig. 2 OCV-SOC fitting curve of the hysteresis effect

According to the fitting curve obtained from the charge and discharge test, when the battery is close to full charge or the battery discharge depth reaches 70% within these two SOC ranges, the hysteresis voltage is relatively large, and the difference in OCV between charge and discharge is the most significant. In order to reduce the impact of hysteresis effects, the average OCV and SOC are taken for polynomial fitting. The mathematical relationship between OCV and SOC is shown in Eq. (9).

$$OCV(S) = 25.951S^6 - 80.987S^5 + 94.934S^4 - 50.856S^3 + 12.351S^2 - 0.657S + 3.449 \tag{9}$$

In Eq. (9), *S* stands for SOC. When fitting the relationship between OCV and SOC based on test data, the fitting accuracy increases with the increase of the fitting order, and the accuracy improvement range of the 7th order becomes smaller after analysis. Considering that the increase of the order will increase the computational complexity, it is more appropriate to choose the 6th-order fitting. In the subsequent temperature test at 25 ℃, the same approach will be used for curve fitting.

2.3. Extended Kalman filtering

Kalman filter is an algorithm that uses the state equation of a linear system to filter the system state through the system input and output observation data. Because it is only applicable to linear systems, its nonlinear system has poor performance. Therefore, in order to make a series of algorithms that can be used in the field of non-linear systems, after continuous research, some scholars have proposed the extended Kalman filtering (EKF) algorithm. When estimating SOC, the EKF algorithm expands the nonlinear system through the Taylor formula, and removes the higher-order terms to linearize the nonlinear system. The state space equation of the nonlinear discrete system is shown in Eq. (10).

$$\begin{cases} x_{k+1} = A_k x_k + B_k u_k + w_k \\ y_k = C_k x_k + D_k u_k + v_k \end{cases} \tag{10}$$

Wherein, x_k and y_k represent system state variables and measurement variables at time k, respectively. u_k is the system input variable at time k. w_k and v_k are process noise and measurement noise, respectively, which are uncorrelated zero mean Gaussian white noise. A_k is the state transition matrix, B_k is the input matrix, C_k is the output matrix, and D_k is the feedforward matrix.

The state vector of the system is shown in Eq. (11).

$$\begin{cases} x_k = (SOC_k, U_{1,k}, U_{2,k})^T \\ u_k = I_{t,k} \end{cases} \tag{11}$$

Combining Eq. (3), Eq. (4) and Eq. (10) can calculate the state transition matrix A_k and the input matrix B_k, as shown in Eq. (12).

$$\begin{cases} \hat{A}_k = \begin{bmatrix} 1 & 0 & 0 \\ 0 & \mathrm{e}^{-\frac{\Delta t}{\tau_1}} & 0 \\ 0 & 0 & \mathrm{e}^{-\frac{\Delta t}{\tau_2}} \end{bmatrix} \\ \hat{B}_k = \begin{bmatrix} -\eta \dfrac{\Delta t}{C} & R_1(1-\mathrm{e}^{-\frac{\Delta t}{\tau_1}}) & R_2(1-\mathrm{e}^{-\frac{\Delta t}{\tau_2}}) \end{bmatrix}^T \end{cases} \tag{12}$$

Since the terminal voltage $U_{L,k}$ in Eq. (4) contains the $U_{OCV,k}$ sub term, although $U_{OCV,k}$ can be expressed as a sixth order polynomial function expression of SOC, there is a non-linear relationship between them. Therefore, conventional Kalman filtering algorithm cannot express $U_{L,k}$ in the form of Eq. (4). The idea of the extended Kalman filtering algorithm is to linearize the nonlinear problem, which uses the Taylor formula to expand the $U_{OCV,k}$ into a linear expression of SOC. The output matrix C_k and the feedforward matrix D_k can be calculated, as shown in Eq. (13).

$$\begin{cases} \hat{C}_k = \left[\dfrac{\mathrm{dU_{ocv}}}{SOC}, -1, -1 \right] \\ \hat{D}_k = -R_0 \end{cases} \tag{13}$$

2.4. Sage Husa extended Kalman filtering

The extended Kalman filtering algorithm converts a nonlinear system into a linear system, it can estimate SOC using the Kalman filter method. However, it ignores the impact of noise changes on SOC estimation, which can cause significant errors. Applying Sage Husa adaptive methods to the EKF algorithm can achieve noise estimation and correction, reducing the impact of noise on SOC estimation. The Sage Husa extended Kalman filtering algorithm is mainly divided into error covariance matrix P_k and noise q_k, r_k, Q_k, and R_k. However, while adjusting Q_k, the error covariance matrix P_k will also be adjusted. Therefore, adaptive methods are often used in practical applications to adjust noise.

After adaptive update of noise parameters, the system state noise q_{k+1}, the covariance matrix of system state noise Q_{k+1}, the system observation noise r_{k+1} and the covariance matrix of system observation noise

R_{k+1} are shown in Eq. (14) to Eq. (17).

$$q_{k+1} = (1-d_k)q_k + d_k G(\hat{x}_{k+1} - A\hat{x}_k - B\hat{u}_k) \tag{14}$$

$$Q_{k+1} = (1-d_k)Q_k + d_k G(K_{k+1}\tilde{y}_{k+1}y_{k+1}^T K_{k+1}^T + \tilde{P}_{k+1/k} - A\tilde{P}_{k+1/k}A^T)G^T \tag{15}$$

$$r_{k+1} = (1-d_k)r_k + d_k(y_{k+1} - C\hat{x}_{k+1} - Du_{k+1}) \tag{16}$$

$$R_{k+1} = (1-d_k)R_k + d_k(\tilde{y}_{k+1}\tilde{y}_{k+1}^T - CP_{k+1/k}C^T) \tag{17}$$

In Eq. (14), $\hat{x}_k$ is the state of the system, *A* is the system state transition matrix, *B* is the control matrix. In Eq. (15), y_{k+1} is the state observation measurement, *G* is the noise driven matrix, $\tilde{P}_{k+1/k}$ is the error covariance matrix of initial prediction. In Eq. (16), *C* is the system measurement matrix, *D* is the system feedforward matrix. d_k is the weighting coefficient, $d_k = (1-b)(1-b^{k+1})$, $n = 0,1,\ldots,k$. d_k is related to the forgetting factor *b* and is the coefficient of the estimator. The value range of *b* is $0.95 \le b \le 0.99$.

2.5. Robust data correction technology

Robust data correction technology is a robust statistic proposed by Huber to eliminate errors in parameter estimation. Its basic principle is to construct a data correction model based on the existing measurement data and instrument information, which can correct the random error contained in the measurement data. It is not sensitive to gross error, so as to obtain accurate data correction results. Its essence is an optimization problem. The objective function is a robust function, which requires the minimum difference between the corrected value and the measured value. The constraint equation is a process model, and the correction value is required to meet the material balance, heat balance, chemical reaction metrological relationship, or other chemical and physical laws. The expression and constraint equation of the dynamic robust data correction model are shown in Eq. (18) and Eq. (19).

$$\min \sum_{k=0}^{\alpha} \rho\left(\frac{\hat{z}_k - z_k}{\delta_k}\right) = \sum_{k=0}^{\alpha} \rho(r_k) \tag{18}$$

$$\text{s.t.}\begin{cases} f\left[\mathrm{d}\hat{z}(\hat{u},t_k)/\mathrm{d}t,\hat{z}(\hat{u},t_k)\right]=0 \\ h\left[\hat{z}(\hat{u},t_k)\right]=0 \\ g\left[\hat{z}(\hat{u},t_k)\right]\geq 0 \end{cases} \tag{19}$$

In Eq. (18), k is the k-th time, α is the current moment, ρ is a robust function. z_k is the measured value vector, $\hat{z}_k$ is the correction value vector, r_k is the relative residual vector. In Eq. (19), f is the differential equation, h is an algebraic equation equality constraint, g is an inequality constraint, including upper and lower bound constraints on variables.

At present, many robust objective functions have been proposed, such as the Cauchy estimation function, Logistic estimation function, Huber estimation function, Fair and Welsch estimation function, etc. These functions have been proven to have certain robustness, and each robust function has its advantages and disadvantages. However, if set adjustment parameters are appropriate, each robust function can achieve the same data correction effect. The simplified expression of the typical Cauchy estimation function is shown in Eq. (20).

$$\rho(r)=\ln(1+\frac{r^2}{c^2}) \tag{20}$$

Wherein, c is an adjustable parameter, which can be selected according to efficiency. r is the relative residual, $r=\left|(z-\hat{z})/\delta\right|$.

To measure the robustness of robust functions, Hampel introduced the concept of influence function in 1986. Suppose there are independent identically distributed variables with samples $\{r_1 \quad r_2 \quad \cdots \quad r_k\}$ obeying distribution ζ and T is an unbiased estimate of parameter θ. That is, $\hat{\theta}=T\left[\zeta(r)\right]$. Then the influence function definition expression is shown in Eq. (21).

$$\phi(r_{r_k})=\lim_{k\to 0}\frac{T\left[(1-k)\zeta+k\delta(r-r_k)\right]-T\left[\zeta\right]}{k} \tag{21}$$

In Eq. (21), $\delta(r-r_k)$ is the Dirac function centered on r_k. If the estimation function is robust, then the influence function is bounded when r_k is infinite. Hampel defines the influence function at r_k as:

$\phi(r_k) = \partial\rho / \partial r_k$. Then the influence function of the simplified Cauchy estimation function is shown in Eq. (22).

$$\phi(r) = \frac{2c^2 r}{c^2 + r^2} \tag{22}$$

Another important function in robust statistics is the joint weight function, which is defined as: $I(r_k) = \phi(r_k) / r_k$. Then the joint weight function of the simplified Cauchy function is shown in Eq. (23).

$$I(r) = \frac{\phi(r)}{r} = \frac{2c^2}{c^2 + r^2} \tag{23}$$

In order to meet the constraint conditions of the model, when the measured value deviates greatly from the true value, the more the objective function needs to adjust the measurement point, the smaller the weight function of the measurement point, and the smaller the weight value of this point in the objective function. The derivation process of the Cauchy robust function is shown in Fig. 3.

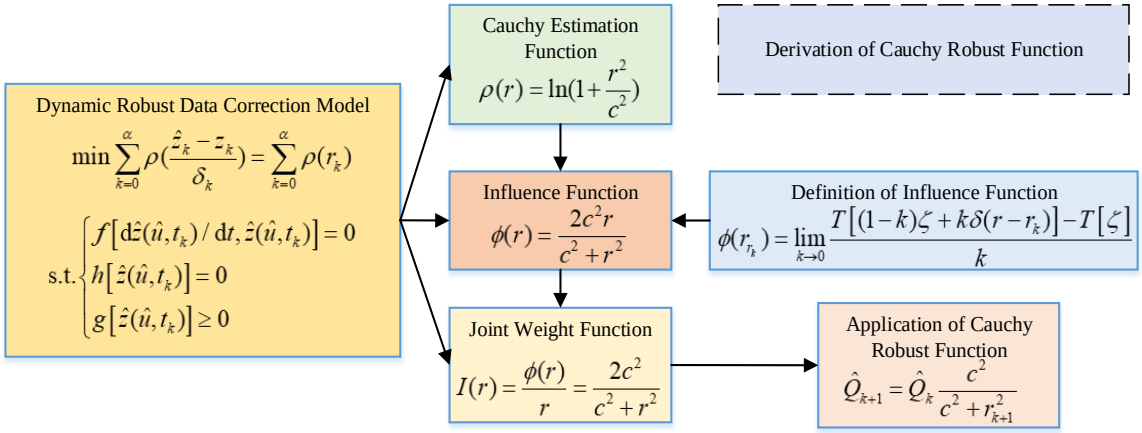

Fig. 3 Derivation process of the Cauchy robust function

By using dynamic robust data correction models, the Cauchy estimation function is used as the robust objective function. After abstracting and simplifying the Cauchy estimation function, the resulting function can be applied to SOC estimation.

2.6. Cauchy robust correction-Sage Husa Extended Kalman Filtering

In order to improve the robustness of the algorithm in a complex noise environment, a robust estimation function with tolerance for large deviation values is needed. With the help of the idea of robust function data

correction, it is applied to the SHEKF algorithm to solve the problem of filter accuracy variation caused by inaccurate system noise estimation. The essence of using the Cauchy robust function to correct the process error is to minimize the difference between the corrected value and the measured value of the objective function. According to the Cauchy robust function, the system state noise covariance matrix *Q* can be modified in real-time to reduce the estimation error. To minimize the objective function, take the relative residual between the filtered prior measurement value $\hat{z}_k^-$ and the actual measurement value z_k as r_k to correct *Q*, which is expressed as: $r_k = \left|(\hat{z}_k^- - z_k)/\delta_k\right|$, wherein, δ_k is the standard deviation of the measured value. The system state noise covariance matrix *Q* equation is shown in Eq. (24).

$$\hat{Q}_{k+1} = \hat{Q}_k \frac{c^2}{c^2 + r_{k+1}^2} \tag{24}$$

Wherein, the value of *c* is a number of the same order of magnitude as r_k. If the order of magnitude is different, it will lead to excessive noise *Q*, making the estimation inaccurate. Because of the system state noise, model error, or inaccurate state estimation, it is unrealistic to accurately estimate a residual of 0 between the state estimation and the actual measurement value. After many iterations, the *Q* value will gradually approach 0. Therefore, it is necessary to set a threshold θ to determine whether to correct *Q*. The equations to determine whether *Q* is corrected are shown in Eq. (25) and Eq. (26).

$$\text{if } \left|r_{k+1}\right| \le \theta, \hat{Q}_{k+1}^c = \hat{Q}_k^c \tag{25}$$

$$\text{else } \hat{Q}_{k+1}^c = \hat{Q}_k^c \frac{c^2}{c^2 + r_{k+1}^2} \tag{26}$$

Because the battery is a highly nonlinear system, the Dual Polarization model established in this paper cannot completely simulate the characteristics of the battery, which leads to some errors in the battery model. When the battery is in use, the battery parameters change dynamically with the SOC value of the battery, especially when the SOC is near 0 or 1, the battery performance changes significantly, resulting in the drastic change of the battery model parameters. In order to suppress the reduction of SOC estimation accuracy caused

by parameter error, the observation noise covariance matrix R can be modified in real-time when the SOC is close to 0 or 1. The specific correction methods of the observed noise covariance matrix R are shown in Eq. (27) to Eq. (29).

$$\text{if} \quad SOC \geq SOC_H, R_k = R_{k0}[1 + G_1(SOC - SOC_H)] \tag{27}$$

$$\text{if} \quad SOC \leq SOC_L, R_k = R_{k0}[1 + G_2(SOC - SOC_L)] \tag{28}$$

$$\text{else} \quad R_k = R_{k0} \tag{29}$$

Wherein, $SOC_H = 0.8$, $SOC_L = 0.2$, G_1 and G_2 are constants, $G_1 = G_2 = 10$.

The specific process of the Cauchy robust correction-adaptive extended Kalman filtering algorithm is:

1) Calculating the system state at time k:

$$\hat{x}_{k+1/k} = A\hat{x}_k + Bu_k + q_k \tag{30}$$

2) Calculating the corrected system state covariance and error covariance at time k:

$$\text{if} \quad \left|r_{k+1}\right| \leq \theta, \hat{Q}^c_{k+1} = \hat{Q}^c_k \tag{31}$$

$$\text{else} \quad \hat{Q}_{k+1} = \hat{Q}_k \frac{c^2}{c^2 + r^2_{k+1}} \tag{32}$$

$$\tilde{P}_{k+1/k} = AP_kA^T + \hat{Q}^c_k \tag{33}$$

3) Calculating the corrected observation noise covariance at time k:

$$\text{if} \quad SOC \geq SOC_H, R_k = R_{k0}[1 + G_1(SOC - SOC_H)] \tag{34}$$

$$\text{if} \quad SOC \leq SOC_L, R_k = R_{k0}[1 + G_2(SOC - SOC_L)] \tag{35}$$

$$\text{else} \quad R_k = R_{k0} \tag{36}$$

4) Calculating the Kalman gain:

$$K_k = \frac{\tilde{P}_{k+1/k}C^T}{C\tilde{P}_{k+1/k}C^T + R_k} \tag{37}$$

Wherein, $C = \left[\frac{\partial U_{oc}}{\partial SOC} \quad -1 \quad -1\right]$.

5) Calculating the system error covariance matrix at k+1 time:

$$\hat{x}_{k+1} = \hat{x}_{k+1/k} + K_k[y_{k+1} - (C\hat{x}_{k+1/k} + Du_k) - r_k] \tag{38}$$

$$P_{k+1} = (I - K_k C)\tilde{P}_{k+1/k} \tag{39}$$

6) Cycling steps (1) to (5) to calculate the value of SOC.

The FFRLS algorithm is used for online parameter identification, and the identified parameters are used for real-time measurement of battery SOC. Since the uncertain system noise will affect the estimation results, an improved CRC-SHEKF algorithm is proposed to estimate the SOC of lithium-ion batteries. It is an adaptive filtering method and the noise correction method can effectively reduce the impact of noise and improve the accuracy of SOC estimation. The frame diagram of estimating the SOC of lithium-ion batteries using the CRC-SHEKF algorithm is shown in Fig. 4.

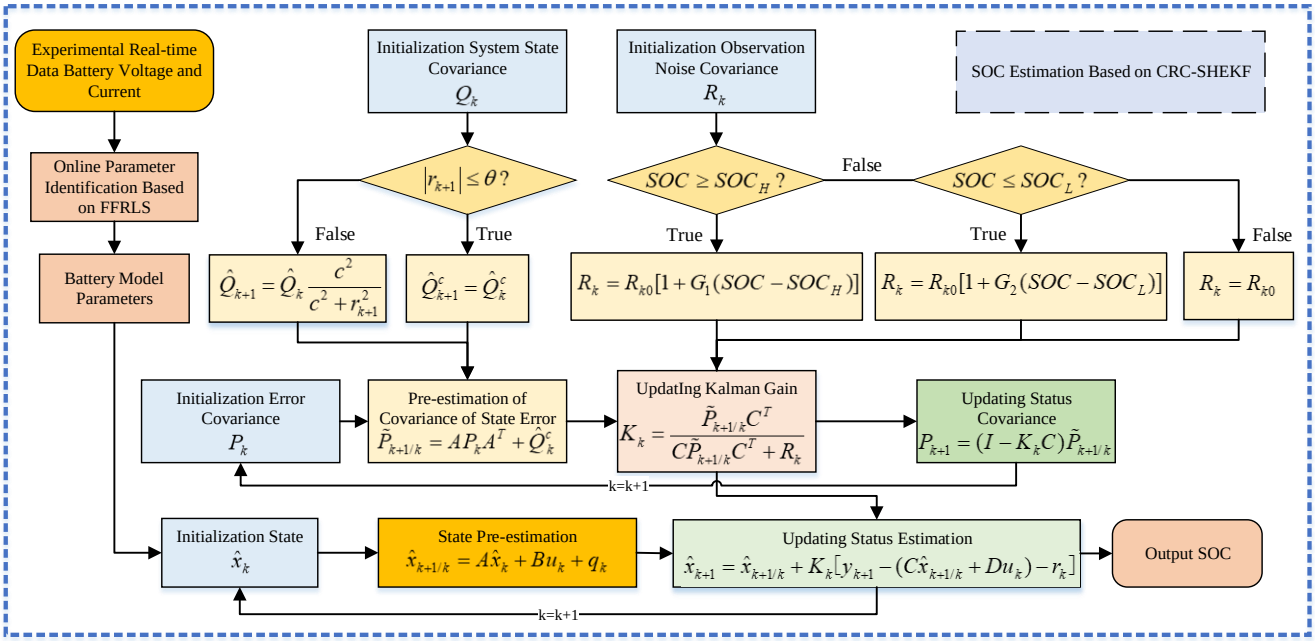

Fig. 4 SOC estimation framework of CRC-SHEKF

First, input the voltage and current data obtained from the experiment, and identify the Dual Polarization model parameters online by the FFRLS algorithm. Then the CRC-SHEKF algorithm reads the identified real-time model parameters and combines the voltage and current data to estimate the battery SOC. In the

CRC-SHEKF algorithm, the system state covariance Q and the observation noise covariance R are selected to correct according to the judgment rules, then the error covariance P and the Kalman gain K are calculated based on the correction values. Finally, the system status is calculated and the SOC value is output.

3. Experimental verification

To verify the reliability of the Dual Polarization model and the superiority of the CRC-SHEKF algorithm, the FFRLS algorithm is used to identify the model parameters. Compare the estimated voltage with the experimental voltage to verify the reliability of the model. The resulting parameters will be passed to the CRC-SHEKF algorithm to estimate the lithium battery SOC. When estimating SOC, the voltage and current under three dynamic working conditions, HPPC, DST, and BBDST, will be used as inputs. The ampere-hour integration method is a classic algorithm for estimating SOC. The calculation formula is the definition of SOC, which estimates SOC by accumulating the amount of charge and discharge during the battery charging and discharging process. This method only records the incoming and outgoing battery power from the outside, which is a theoretical value, and ignores the changes in the internal state of the battery. This article takes the SOC theoretical calculation value of the ampere-hour integration method as the true value and compares it with the estimated values of other algorithms. The output SOC estimated value is compared with the actual SOC value to verify the accuracy of the CRC-SHEKF algorithm. In this paper, mean absolute error (MAE), root mean square error (RMSE), maximum error (MAX), and computing time are selected as evaluation indexes.

3.1. Experimental test platform

The experimental platform is composed of a charge-discharge tester, an upper computer, and other experimental equipment. The type of charge-discharge tester is CT-4016-5V100A-NTFA. The type of ternary lithium battery used in the test is BTS200-100-104, the rated capacity is 70 Ah, and the actual capacity is 62.76 Ah. The test instrument measures the U/I/T signal in real-time through TCP/IP and transmits the data to the upper computer. The experimental test platform is shown in Fig. 5.

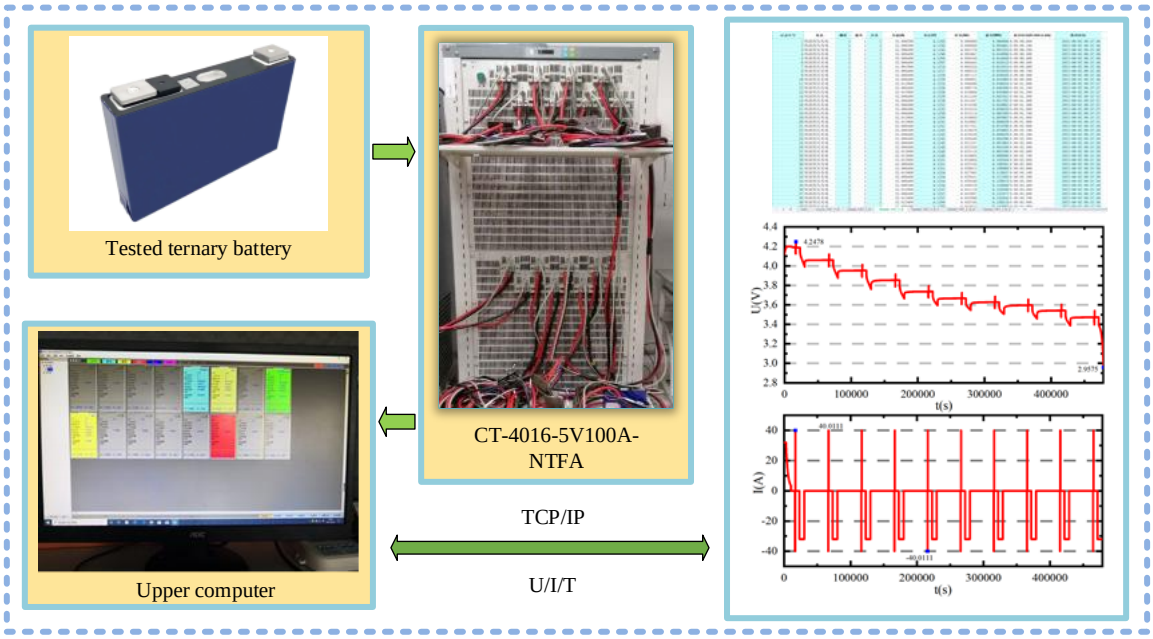

Fig. 5 The experimental test platform

3.2. Model validation

The voltage and current data under HPPC working conditions at 15℃ are used as input and the FFRLS algorithm is used for online parameter identification of the Dual Polarization model. The reliability of the Dual Polarization model is verified by comparing the actual voltage obtained from the experiment with the simulated voltage output from the FFRLS algorithm. The voltage comparison under HPPC working conditions is shown in Fig. 6.

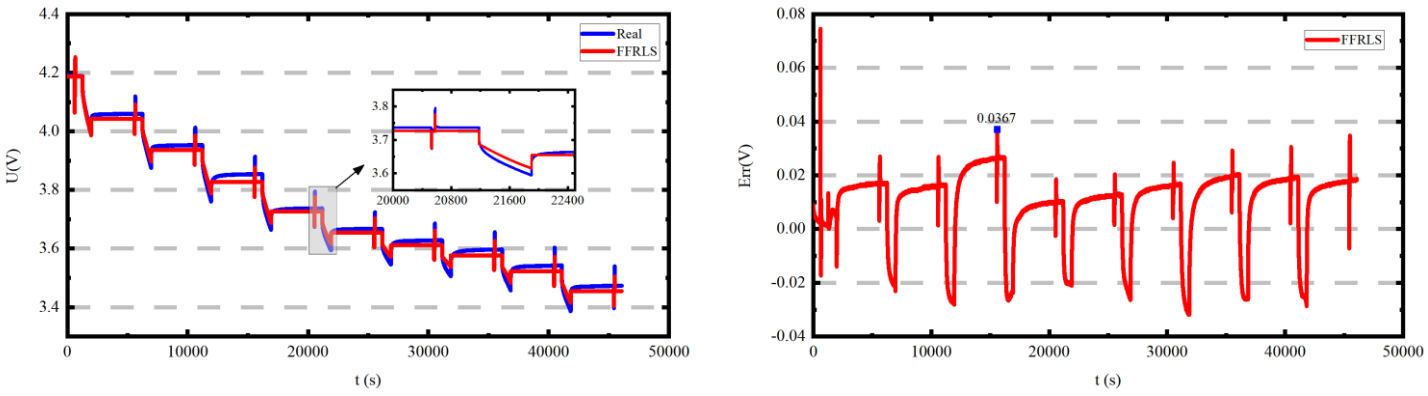

(a) Real voltage and simulation voltage

(b) Voltage simulation error

Fig. 6 Voltage comparison under HPPC working conditions

According to Fig. 6, in the initial stage, the error is significantly greater due to the convergence of the

algorithm and the influence of the initial value. In each cycle, the simulation error of the sudden change of current, that is, the charge and discharge part of the battery, is relatively large, which is related to the intense chemical reaction inside the lithium battery, and the simulation results are very good in the remaining stages. The MAE and RMSE of the FFRLS algorithm are 0.99% and 1.65%, respectively. Without regard to the error at the convergence stage of the algorithm, the maximum error is 0.0367V. The experimental results show that the FFRLS algorithm can effectively characterize the Dual Polarization model, and obtain more accurate online parameter identification results for subsequent SOC estimation.

3.3. Analysis of SOC estimation results under complex working conditions

To validate the proposed CRC-SHEKF algorithm, its accuracy needs to be verified under different complex working conditions, including HPPC, DST, and BBDST. At the same time, to verify the adaptability of the proposed algorithm to temperature, different operating conditions data of 15℃ and 25℃ were used for comparison. The HPPC working conditions refer to hybrid pulse power characterization, which can well reflect the dynamic characteristics of the battery during operation. The DST working conditions are a complex condition that evolved from the operating conditions of federal cities in the United States, which includes the continuous charging and discharging process of lithium batteries. The BBDST working conditions come from the real data collection of Beijing's public transportation dynamic testing, which includes data from various operations such as starting, coasting, acceleration, and rapid acceleration. It has authenticity and dynamism, while the actual application conditions of high-power lithium batteries are complex and variable. Therefore, using BBDST experimental data to verify the algorithm is even more convincing.

3.3.1. Analysis of the results under HPPC working conditions

To verify the superiority of the CRC-SHEKF algorithm, the SOC estimates of the EKF, SHEKF, and CRC-SHEKF algorithms were compared. The comparison of SOC estimation results and the comparison of SOC estimation errors of different algorithms under HPPC working conditions are shown in Fig. 7.

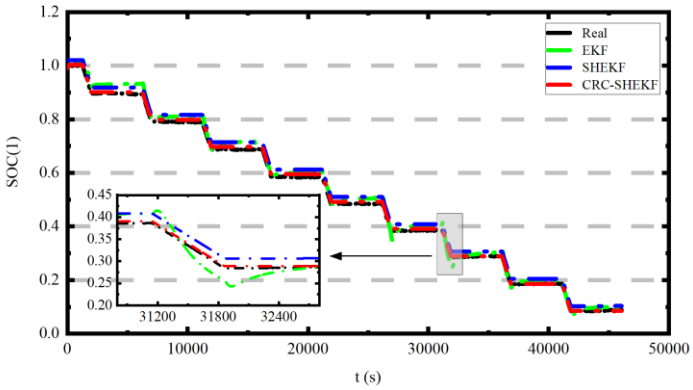

(a) SOC estimation results at 15℃

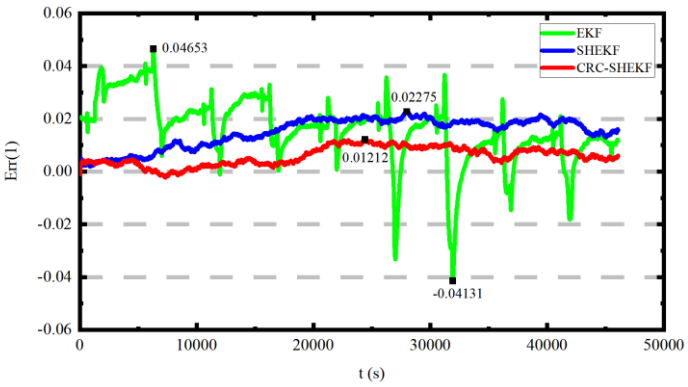

(b) SOC estimation error at 15℃

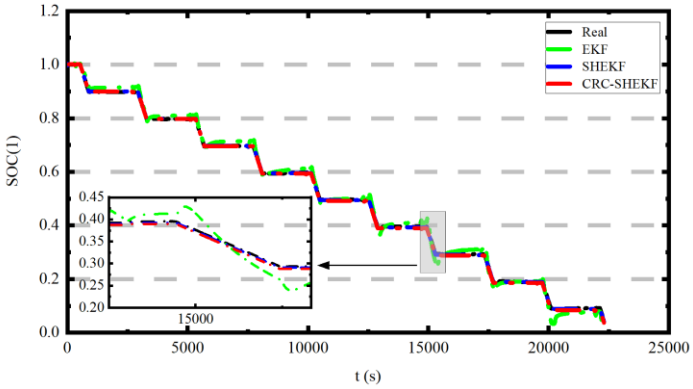

(c) SOC estimation results at 25℃

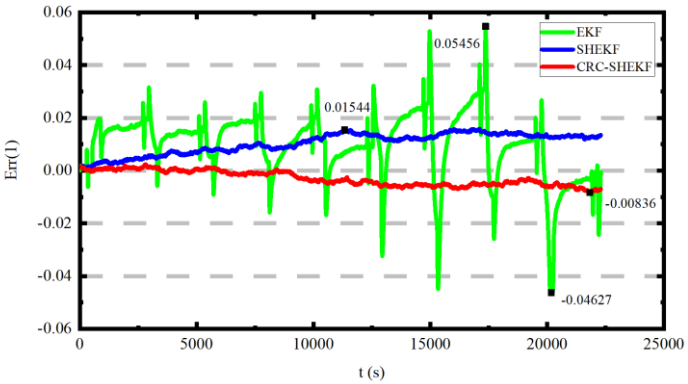

(d) SOC estimation error at 25℃

Fig. 7 SOC comparison under HPPC working conditions

According to Fig. 7a, the EKF algorithm exhibits significant fluctuations in SOC at stages 0.9, 0.4, and 0.3, and is not as stable as the SHEKF and CRC-SHEKF algorithms. The SOC estimation value of the CRC-SHEKF algorithm is closer to the true value than that of the SHEKF algorithm. According to Fig. 7b, the maximum error of the CRC-SHEKF algorithm is 0.01212, which is reduced by 0.03441 and 0.01063 compared to the EKF and SHEKF algorithms, respectively. Tab. 2 shows the indicators of different algorithms under HPPC working conditions.

Tab. 2 Indicators of different algorithms under HPPC working conditions

Temperature	Algorithm	MAE	RMSE	MAX	Computing time(s)
15℃	EKF	0.01632	0.01858	0.04653	11.045
	SHEKF	0.01502	0.01602	0.02275	15.374
	CRC-SHEKF	0.00579	0.00728	0.01212	12.653
25℃	EKF	0.01377	0.01612	0.05456	5.495
	SHEKF	0.01107	0.01242	0.01544	7.654
	CRC-SHEKF	0.00334	0.00414	0.00836	6.504

According to Tab. 2, the MAE, RMSE, and MAX of the SHEKF algorithm are all smaller than those of the EKF algorithm, due to the Sage Husa adaptive noise method. The CRC-SHEKF algorithm performs best due to noise correction, which makes the estimation process more in line with the real situation. Comparing the computation time of the three methods, the SHEKF algorithm takes longer than the EKF algorithm due to its iterative calculation of uncertain random noise. The Cauchy robust correction process uses judgment statements to correct noise, simplifies the iterative calculation process, and has a shorter calculation time than the SHEKF algorithm. Under the HPPC working conditions, the CRC-SHEKF algorithm can reduce the impact of random noise and improve the accuracy of SOC estimation. However, validation under one working condition does not necessarily demonstrate the superiority of the algorithm, and validation needs to be conducted under different working conditions.

3.3.2. Analysis of the results under DST working conditions

The comparison of SOC estimation results and the comparison of SOC estimation errors of different algorithms under DST working conditions are shown in Fig. 8.

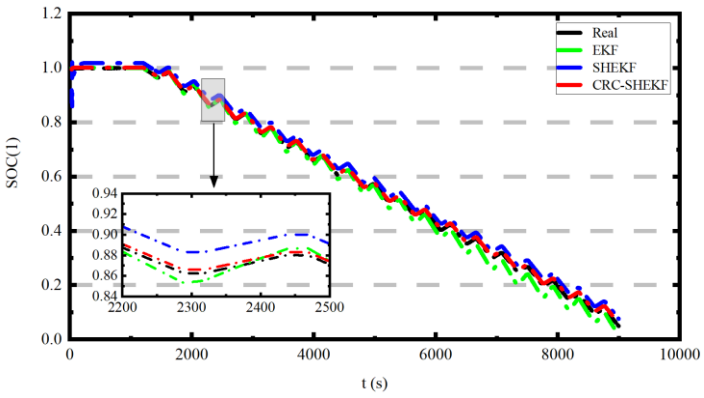

(a) SOC estimation results at 15℃

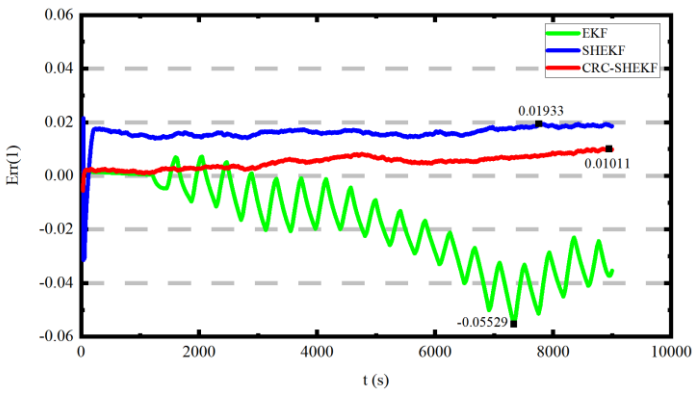

(b) SOC estimation error at 15℃

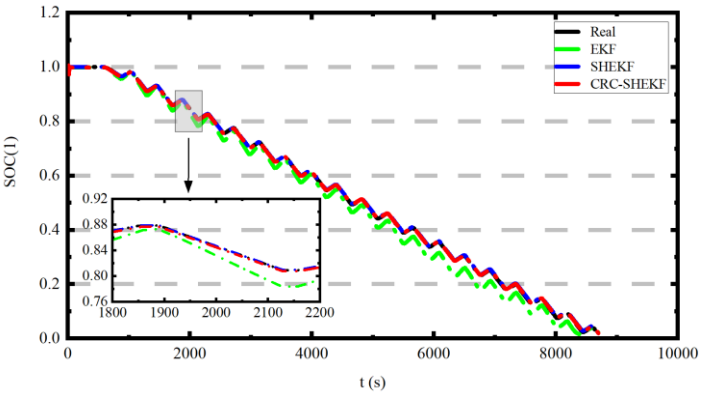

(c) SOC estimation results at 25℃

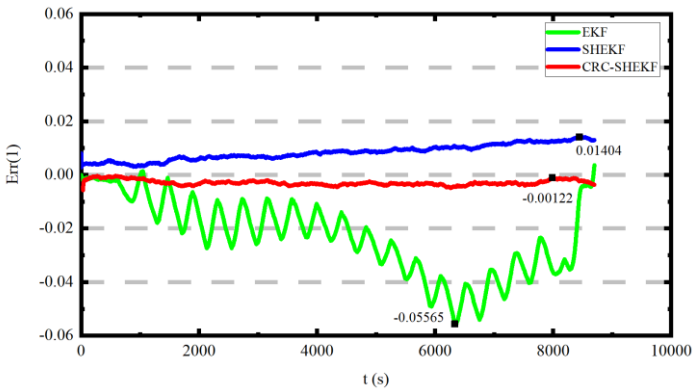

(d) SOC estimation error at 25℃

Fig. 8 SOC comparison under DST working conditions

According to Fig. 8, the EKF algorithm has a significant estimation error when the SOC is below 0.5. The CRC-SHEKF algorithm has a faster convergence time and a minimum maximum error. Tab. 3 shows the indicators of different algorithms under DST working conditions.

Tab. 3 Indicators of different algorithms under DST working conditions

Temperature	Algorithm	MAE	RMSE	MAX	Computing time(s)
15℃	EKF	0.01765	0.02365	0.05529	4.244
	SHEKF	0.01584	0.01683	0.01993	11.624
	CRC-SHEKF	0.00499	0.00851	0.01011	4.468
25℃	EKF	0.02306	0.02707	0.05565	4.056
	SHEKF	0.01327	0.01548	0.01404	11.232
	CRC-SHEKF	0.00491	0.00556	0.00122	4.678

According to Tab. 3, under DST working conditions, the CRC-SHEKF algorithm has the best performance in all indicators and has the same experimental results as HPPC.

3.3.3. Analysis of the results under BBDST working conditions

The comparison of SOC estimation results and the comparison of SOC estimation errors of different algorithms under BBDST working conditions are shown in Fig. 9.

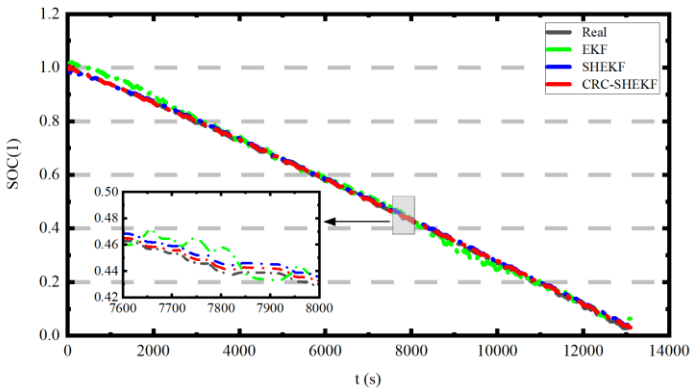

(a) SOC estimation results at 15℃

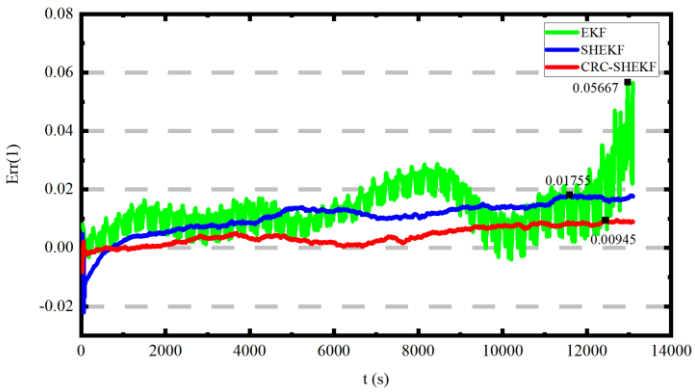

(b) SOC estimation error at 15℃

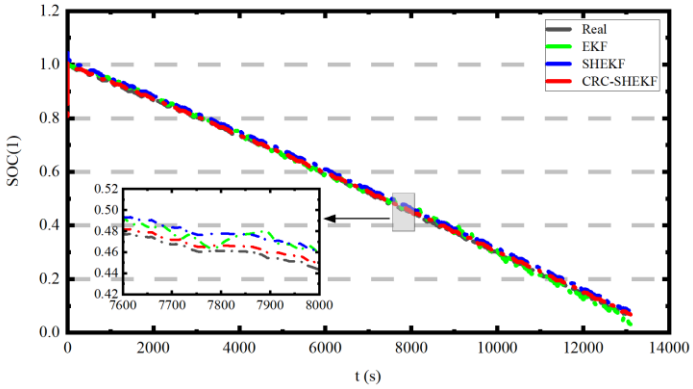

(c) SOC estimation results at 25℃

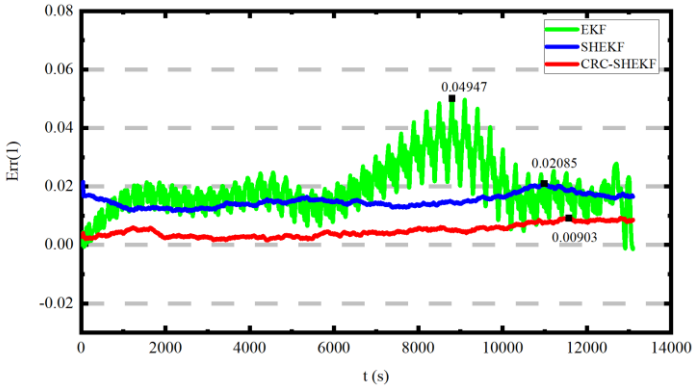

(d) SOC estimation error at 25℃

Fig. 9 SOC comparison under BBDST working conditions

According to Fig. 9, the EKF algorithm has significant errors during the SOC stages of 1.0 to 0.8, 0.4 to 0.2, and the end stage, due to the influence of random noise in the system. The CRC-SHEKF algorithm has a smaller convergence time, faster convergence speed, and smaller error. The indicators of different algorithms under BBDST working conditions are shown in Tab. 4.

Tab. 4 Indicators of different algorithms under BBDST working conditions

Temperature	Algorithm	MAE	RMSE	MAX	Computing time(s)
15℃	EKF	0.01364	0.01572	0.05567	4.279
	SHEKF	0.01056	0.01196	0.01755	10.873
	CRC-SHEKF	0.00392	0.00716	0.00945	4.839
25℃	EKF	0.01897	0.02075	0.04947	4.298
	SHEKF	0.01511	0.01627	0.02085	10.615
	CRC-SHEKF	0.00481	0.00557	0.00903	4.881

The comparison of various indicators of different algorithms under three working conditions is shown in Fig. 10.

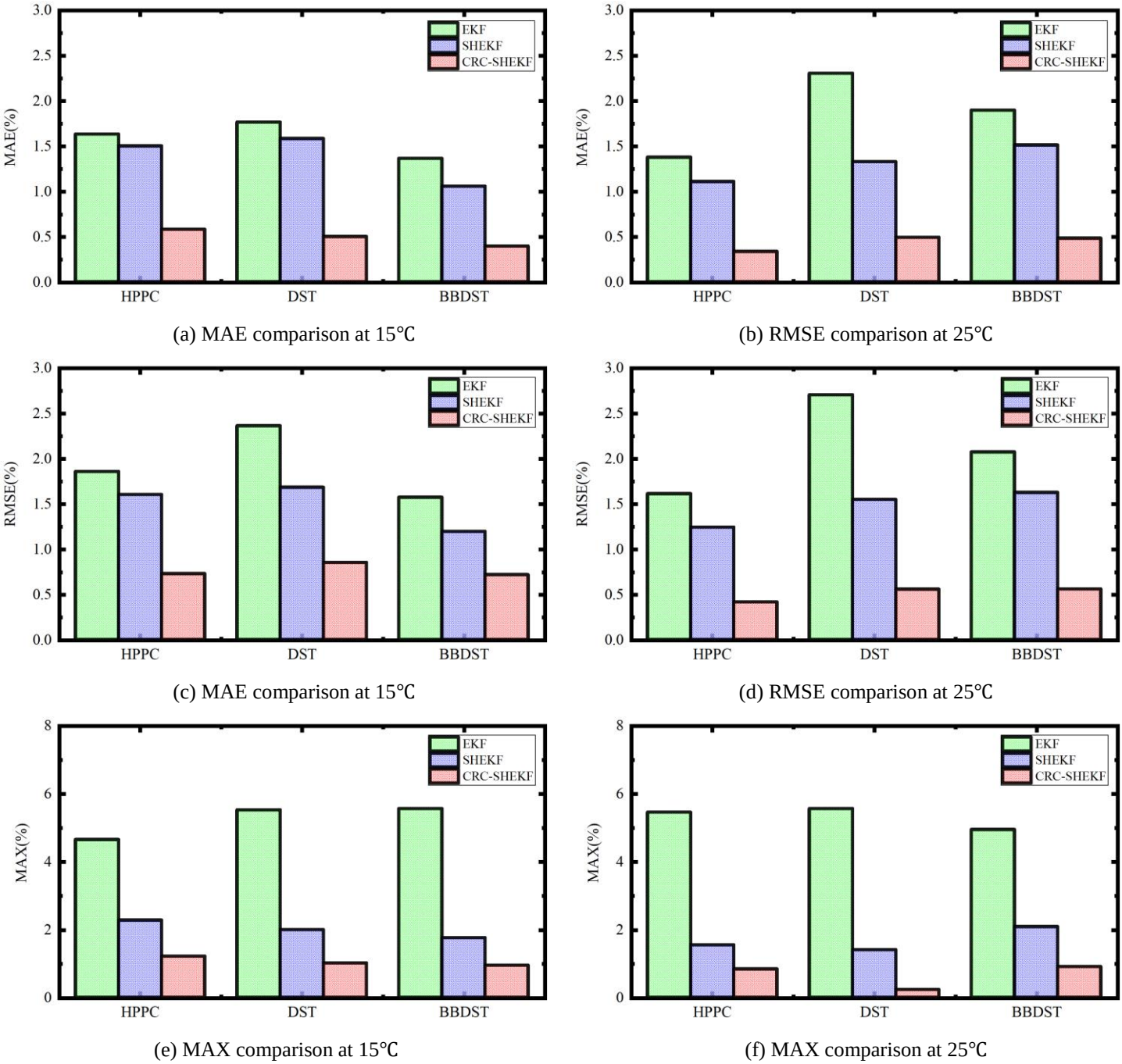

(a) MAE comparison at 15℃

(b) RMSE comparison at 25℃

(c) MAE comparison at 15℃

(d) RMSE comparison at 25℃

(e) MAX comparison at 15℃

(f) MAX comparison at 25℃

Fig. 10 Indicators comparison under different working conditions

According to Fig. 10, it can be intuitively seen that under different complex working conditions, the various indicators of the CRC-SHEKF algorithm are optimal and suitable for different complex working conditions, and have good temperature adaptability. From this, it can be concluded that the Cauchy robust correction method can reduce the impact of random noise, and the proposed CRC-SHEKF algorithm has strong adaptability and higher accuracy.

4. Conclusion

In order to solve the problem of inaccurate noise estimation of nonlinear systems, an improved Cauchy robust correction-Sage Husa extended Kalman filtering (CRC-SHEKF) algorithm is proposed to estimate the SOC of lithium-ion batteries. Firstly, the FFRLS algorithm is used to identify the model parameters of the Dual Polarization model online. To reduce the impact of hysteresis effects, the average OCV and SOC are taken for polynomial fitting. The CRC-SHEKF algorithm reads the real-time model parameter values, combines the Cauchy robust function with the Sage Husa method to modify the filtering state noise covariance matrix Q, and real-time corrects the noise covariance matrix R when the SOC approaches 0 or 1. The CRC-SHEKF algorithm exhibits better robustness and achieves high-precision SOC estimation for lithium-ion batteries. The experimental results show that under various complex working conditions, the improved CRC-SHEKF algorithm has smaller estimation errors. MAE, RMSE, and MAX are the smallest compared to EKF and SHEKF under three working conditions HPPC, DST, and BBDST. This effectively suppresses the problem of estimation accuracy degradation caused by unknown statistical features of system noise or battery model errors, while improving the stability and accuracy of the algorithm. Meanwhile, the algorithm has strong adaptability to temperature and short calculation time. It has good practical application value and provides a reference for the application of lithium battery condition monitoring.

Acknowledgments

The work was supported by the National Natural Science Foundation of China (No.62173281,61801407).

References

[1]. Liu, X., et al., *Regrouping strategy of retired batteries considering SOC consistency*. Energy Reports, 2022. 8: p. 218-228.

[2]. Saleh, S. A., et al., *On the Factors Affecting Battery Unit Contributions to Fault Currents in Grid-Connected Battery Storage Systems*. IEEE Transactions on Industry Applications, 2022. 58(3): p. 3019-3028.

[3]. Huang, C. S., Z. Y. Cheng, & M. Y. Chow, *A Robust and Efficient State-of-Charge Estimation Methodology for Serial-Connected Battery Packs: Most Significant Cell Methodology*. IEEE Access, 2021. 9: p. 74360-74369.

[4]. Tang, A. H., et al., *A multi-model real covariance-based battery state-of-charge fusion estimation method for electric vehicles using ordered weighted averaging operator*. International Journal of Energy Research, 2022. 46(12): p.

17273-17284.
[5]. Cao, Y., & J. A. Abu Qahouq, *Hierarchical SOC Balancing Controller for Battery Energy Storage System*. IEEE Transactions on Industrial Electronics, 2021. 68(10): p. 9386-9397.
[6]. Cui, Z. H., et al., *A comprehensive review on the state of charge estimation for lithium-ion battery based on neural network*. International Journal of Energy Research, 2022. 46(5): p. 5423-5440.
[7]. Yun, S. T., & S. H. Kong, *Data-Driven In-Orbit Current and Voltage Prediction Using Bi-LSTM for LEO Satellite Lithium-Ion Battery SOC Estimation*. IEEE Transactions on Aerospace and Electronic Systems, 2022. 58(6): p. 5292-5306.
[8]. Wang, S. L., et al., *An improved coulomb counting method based on dual open-circuit voltage and real-time evaluation of battery dischargeable capacity considering temperature and battery aging*. International Journal of Energy Research, 2021. 45(12): p. 17609-17621.
[9]. Liu, D. L., et al., *A novel fuzzy-extended Kalman filter-ampere-hour (F-EKF-Ah) algorithm based on improved second-order PNGV model to estimate state of charge of lithium-ion batteries*. International Journal of Circuit Theory and Applications, 2022. 50(11): p. 3811-3826.
[10]. Bavand, A., et al., *Online Estimations of Li-Ion Battery SOC and SOH Applicable to Partial Charge/Discharge*. IEEE Transactions on Transportation Electrification, 2022. 8(3): p. 3673-3685.
[11]. Tian, J. P., et al., *Electrode ageing estimation and open circuit voltage reconstruction for lithium ion batteries*. Energy Storage Materials, 2021. 37: p. 283-295.
[12]. Lin, J. S., et al., *Algorithm of BPNN-UKF based on a fusion model for SOC estimation in lithium-ion batteries*. IET Power Electronics, 2023. 16(5): p. 856-867.
[13]. Xing, L. K., L. Y. Ling, & X. Y. Wu, *Lithium-ion battery state-of-charge estimation based on a dual extended Kalman filter and BPNN correction*. Connection Science, 2022. 34(1): p. 2332-2363.
[14]. Li, J. B., et al., *Joint estimation of state of charge and state of health for lithium-ion battery based on dual adaptive extended Kalman filter*. International Journal of Energy Research, 2021. 45(9): p. 13307-13322.
[15]. Li, J. B., et al., *A novel battery state estimation model based on unscented Kalman filter*. Ionics, 2021. 27(6): p. 2673-2683.
[16]. Sylvestrin, G. R., H. F. Scherer, & O. H. Ando, *Experimental Validation of State of Charge Estimation by Extended Kalman Filter and Modified Coulomb Counting*. IEEE Latin America Transactions, 2022. 20(11): p. 2395-2403.
[17]. Zhou, J., et al., *Research on the SOC Estimation Algorithm of Combining Sliding Mode Observer With Extended Kalman Filter*. Proceedings of the Chinese Society of Electrical Engineering, 2021. 41(2): p. 692-702.
[18]. Oh, H., J. Jeon, & S. Park, *Effects of Battery Model on the Accuracy of Battery SOC Estimation Using Extended Kalman Filter under Practical Vehicle Conditions Including Parasitic Current Leakage and Diffusion Of Voltage*. International Journal of Automotive Technology, 2021. 22(5): p. 1337-1346.
[19]. Dang, L. J., et al., *Multi-kernel correntropy based extended Kalman filtering for state-of-charge estimation*. ISA Transactions, 2022. 129: p. 271-283.
[20]. Liu, B. L., et al., *An improved adaptive cubature H-infinity filter for state of charge estimation of lithium-ion battery*. Journal of Power Electronics, 2021. 21(10): p. 1520-1529.
[21]. Huang, C., et al., *State of charge estimation of li-ion batteries based on the noise-adaptive interacting multiple model*. Energy Reports, 2021. 7: p. 8152-8161.
[22]. Zhang, Z. Q., B. Q. Xue, & J. M. Fan, *Noise Adaptive Moving Horizon Estimation for State-of-Charge Estimation of Li-Ion Battery*. IEEE Access, 2021. 9: p. 5250-5259.
[23]. Wu, Y., et al., *Research on life cycle SOC estimation method of lithium-ion battery oriented to decoupling temperature*. Energy Reports, 2022. 8: p. 4182-4195.
[24]. Yue, W., et al., *A nonlinear fractional-order H-infinity observer for SOC estimation of battery pack of electric vehicles*. Proceedings of The Institution of Mechanical Engineers Part D-Journal of Automobile Engineering, 2021. 235(9): p. 2484-2495.
[25]. Liu, Y. Y., et al., *A novel adaptive H-infinity filtering method for the accurate SOC estimation of lithium-ion batteries*

based on optimal forgetting factor selection. International Journal of Circuit Theory and Applications, 2022. 50(10): p. 3372-3386.
[26]. Wang, L. M., et al., *State of Charge Estimation of Lithium-Ion Based on VFFRLS-Noise Adaptive CKF Algorithm*. Industrial & Engineering Chemistry Research, 2022. 61(22): p. 7489-7503.
[27]. Ali, M. U., et al., *An adaptive state of charge estimator for lithium-ion batteries*. Energy Science & Engineering, 2022. 10(7): p. 2333-2347.
[28]. Chen, P. Y., et al., *Evaluation of Various Offline and Online ECM Parameter Identification Methods of Lithium-Ion Batteries in Underwater Vehicles*. ACS Omega, 2022. 7(34): p. 30504-30518.
[29]. Jin, Y. Z., C. L. Su, & S. C. Luo, *Improved Algorithm Based on AEKF for State of Charge Estimation of Lithium-ion Battery*. International Journal of Automotive Technology, 2022. 23(4): p. 1003-1011.
[30]. Zhu, L., et al., *Research on a battery SOC prediction method based on the RLS-DLUKF algorithm*. Energy Storage Science and Technology, 2021. 10(3): p. 1137-1144.
[31]. Ren, Z., et al., *A comparative study of the influence of different open circuit voltage tests on model-based state of charge estimation for lithium-ion batteries*. International Journal of Energy Research, 2021. 45(9): p. 13692-13711.
[32]. Fu, S. Y., et al., *Study of impacts of parameters identification methods on model-based state estimation for LiFePO4 battery*. Ionics, 2022. 28(7): p. 3321-3339.
[33]. Li, J. B., et al., *SOC estimation for lithium-ion batteries based on a novel model*. IET Power Electronics, 2021. 14(13): p. 2249-2259.
[34]. Adaikkappan, M., & N. Sathiyamoorthy, *A real time state of charge estimation using Harris Hawks optimization-based filtering approach for electric vehicle power batteries*. International Journal of Energy Research, 2022. 46(7): p. 9293-9309.
[35]. Huang, Z. J., Y. S. Fang, & J. J. Xu, *SOC ESTIMATION OF Li-ION BATTERY BASED ON IMPROVED EKF ALGORITHM*. International Journal of Automotive Technology, 2021. 22(2): p. 335-340.
[36]. Xia, B. Z., et al., *Online Parameter Identification and State of Charge Estimation of Lithium-Ion Batteries Based on Forgetting Factor Recursive Least Squares and Nonlinear Kalman Filter*. Energies, 2018. 11(1).
[37]. Wadi, A., et al., *An Invariant Method for Electric Vehicle Battery State-of-Charge Estimation Under Dynamic Drive Cycles*. IEEE Access, 2023. 11: p. 8663-8673.
[38]. Takyi-Aninakwa, P., et al., *A strong tracking adaptive fading-extended Kalman filter for the state of charge estimation of lithium-ion batteries*. International Journal of Energy Research, 2022. 46(12): p. 16427-16444.
[39]. Wang, T. H., et al., *Hierarchical Power Allocation Method Based on Online Extremum Seeking Algorithm for Dual-PEMFC/Battery Hybrid Locomotive*. IEEE Transactions on Vehicular Technology, 2021. 70(6): p. 5679-5692.
[40]. Yang, R. X., R. Xiong, & W. X. Shen, *On-board Diagnosis of Soft Short Circuit Fault in Lithium-ion Battery Packs for Electric Vehicles Using an Extended Kalman Filter*. CSEE Journal of Power and Energy Systems, 2022. 8(1): p. 258-270.
[41]. Liu, Z., et al., *State of charge estimation for Li-ion batteries based on iterative Kalman filter with adaptive maximum correntropy criterion*. Journal of Power Sources, 2023. 580: p. 233282.
[42]. Yang, C., Z. Yang, & Z. Deng, *Robust weighted state fusion Kalman estimators for networked systems with mixed uncertainties*. Information Fusion, 2019. 45: p. 246-265.